Lasers Med Sci (2012) 27:903–916
DOI 10.1007/s10103-011-1010-2

ORIGINAL ARTICLE

Effects of LED phototherapy on bone defects grafted with MTA, bone morphogenetic proteins and guided bone regeneration: a Raman spectroscopic study

Antonio L. B. Pinheiro · Luiz G. P. Soares · Maria Cristina T. Cangussú · Nicole R. S. Santos · Artur Felipe S. Barbosa · Landulfo Silveira Júnior

Received: 5 May 2011 / Accepted: 23 September 2011 / Published online: 21 October 2011

Abstract We studied peaks of calcium hydroxyapatite (CHA) and protein and lipid CH groups in defects grafted with mineral trioxide aggregate (MTA) treated or not with LED irradiation, bone morphogenetic proteins and guided bone regeneration. A total of 90 rats were divided into ten groups each of which was subdivided into three subgroups (evaluated at 15, 21 and 30 days after surgery). Defects were irradiated with LED light (wavelength 850±10 nm) at 48-h intervals for 15 days. Raman readings were taken at the surface of the defects. There were no statistically significant differences in the CHA peaks among the nonirradiated defects at any of the experimental time-points. On the other hand, there were significant differences between the defects filled with blood clot and the irradiated defects at all time-points ($p<0.001$, $p=0.02$, $p<0.001$). There were significant differences between the mean peak CHA in nonirradiated defects at all the experimental time-points ($p<0.01$). The mean peak of the defects filled with blood clot was significantly different from that of the defects filled with MTA ($p<0.001$). There were significant differences between the defects filled with blood clot and the irradiated defects ($p<0.001$). The results of this study using Raman spectral analysis indicate that infrared LED light irradiation improves the deposition of CHA in healing bone grafted or not with MTA.

Keywords Biomaterial · Bone repair · Light emitting diode · MTA

A. L. B. Pinheiro (✉) · L. G. P. Soares · N. R. S. Santos · A. F. S. Barbosa
Center of Biophotonics, School of Dentistry,
Federal University of Bahia,
Av. Araújo Pinho, 62, Canela,
Salvador, BA CEP 40110-150, Brazil
e-mail: albp@ufba.br

A. L. B. Pinheiro · L. S. Júnior
Universidade Camilo Castelo Branco Núcleo do Parque Tecnológico de São José dos Campos,
São José dos Campos, SP, Brazil

A. L. B. Pinheiro
Instituto Nacional de Ciência e Tecnologia de Óptica e Fotônica,
São Carlos, SP, Brazil

M. C. T. Cangussú
Oral Epidemiology and Public Health, School of Dentistry,
Federal University of Bahia,
Av. Araujo Pinho, 62, Canela,
Salvador, BA, Brazil

Introduction

It has been shown in various in vitro and in vivo models that near-infrared light irradiation stimulates the photoacceptor cytochrome *c* oxidase, resulting in increased energy metabolism and production, stimulation of mitochondrial oxidative metabolism, and acceleration of tissue repair [1]. Bone is a complex, highly organized, very dynamic, specialized connective tissue, hard, rigid and strong. Microscopically it shows few metabolically active cells, hematopoietic elements of bone marrow and a large amount of intercellular substance formed from collagen fibers and stiffening substances [2]. It is composed of organic and inorganic elements [2, 3]. The latter consist primarily of calcium phosphate and calcium carbonate, with small quantities of magnesium, fluorine, and sodium. The mineral crystals form hydroxyapatite, which precipitates in an orderly arrangement around the collagen fibers of the osteoid. This latter is the nonmineralized organic matrix

secreted by osteoblasts and is composed of 90% type I collagen and 10% ground substance. The mineralization of osteoid by inorganic mineral salts gives bone its strength and rigidity. Its initial calcification normally occurs within a few days of its secretion but is completed over several months [3, 4].

The choice of bone graft is affected by anatomical, histological, and biochemical factors. In addition, several physiological properties of bone grafts, such as osteogenesis, osteoinduction and osteoconduction, directly affect the success or failure of graft incorporation [4]. Alloplasts are synthetic grafting materials used to help the repair of bone defects and to enhance bone ingrowth. Their chemical composition, physical form, and surface configuration, and differences in their porosity, geometry, solubility and density, determine their bioresorbability [5–7]. The treatment of bone defects using biomaterials has been extensively studied in the dental field [8]. Bone loss may be a result of several pathologies, trauma or surgical procedures. These aspects have led to extensive studies worldwide on the process of bone repair. Several techniques for the correction of bone defects have been proposed, including the use of several types of grafts, membranes and the combination of the two techniques [8].

Mineral trioxide aggregate (MTA) is a bacteriostatic powder aggregate containing 65% calcium oxide, 21% calcium silicate, 5% ferric oxide, 4% calcium aluminate, 2.5% calcium sulfates, 2% magnesium oxide, and 0.5% sodium and potassium oxide (pH 12.5). It is not cytotoxic and produces a good biological response. It stimulates tissue repair by increasing cellular adhesion, growth and proliferation at its surface. Unlike other cements, which demand a completely dry field, MTA is indicated when moisture control is inadequate. Under such conditions it shows no loss of its properties and it is not reabsorbed. Previous histological studies have indicated that new bone or cementum is formed adjacent to MTA when it is placed in contact with the periodontal tissue or in artificial bone defects [9–15].

Bone morphogenetic proteins (BMPs) also have osteoinductive characteristics, and inorganic materials such as bone substitutes cause no osteoinduction due to a lack of the proteins required for induction of stem cell differentiation. Calcium phosphates have a high affinity for proteins (such as BMPs) [5]. Guided bone regeneration (GBR) is a procedure based on the guided tissue regeneration technique which is a periodontal surgical procedure that has been in clinical use for more than a decade. Its principles are based on the selective permeability provided by the membranes for the isolation of tissues not essential for bone repair. The use GBR with biomaterials is considered to be beneficial for the healing of bone defects [6, 8, 15].

LEDs show a relatively narrow emission spectrum that may be optimally tuned to correspond to the requirements of a treatment eliminating unnecessary wavelengths from a particular therapy. Their light intensity can be adjusted and they produce high light levels with low radiant heat output and maintain useful output for long periods of time. LED-based devices may provide a homogeneous light dose at optimal intensity [1]. While lasers provide tissue stimulation, which increases cellular activity during wound healing, they have the limitation of a restricted wavelength. Lasers cannot easily produce wavelength combinations optimal for wound healing. The size of wounds that may be treated by the small beam width of laser is also limited. In contrast, the spectral composition of LEDs can be controlled and they may be arranged in flat arrays of all sizes for the treatment of both small and large areas. LEDs offer an effective alternative to the use of conventional light sources [1].

Despite the growing number of successful applications of LED phototherapy (LPT) in many fields, its use in bone repair has not yet been well studied. We were unable to find previous studies on the use of combinations of LED light and biomaterials. LEDs have been used both experimentally and clinically, and beneficial effects of their use have been reported elsewhere [16–21]. It is known that some wavelengths have the ability to stimulate cell proliferation including that of fibroblasts, and these cells have the capacity to secrete collagen, a main organic component observed during bone repair [8, 21–37]. Many techniques are used to improve the bone healing, including light therapies. Several studies have demonstrated that irradiation with near-Infrared wavelengths can improve bone repair due to its high penetration into tissues compared to visible light [8, 21–37]. Although the use of LPT for bone healing has been growing steadily, and several studies have demonstrated positive results in the healing of bone tissue [8, 21–37], there are to date few reports of the use of combinations of LED light and MTA [37].

Raman spectroscopy is a relatively simple, reproducible and nondestructive vibrational spectroscopic technique that may be used to optically probe the molecular changes associated with diseased tissues. Only small amounts of material (micrograms to nanograms) with minimal sample preparation are required. In addition, the technique provides information at the molecular level, allowing investigation of functional groups, bonding types, and molecular conformations. Spectral bands in vibrational spectra are molecule-specific and provide direct information about the biochemical composition. These bands are relatively narrow, easy to resolve, and sensitive to molecular structure, conformation, and environment [38]. The Raman spectrum of bone shows prominent vibrational bands related to tissue composition. Some main Raman bands for tissues are at 862, 958, 1,070,

1,270, 1,326, 1,447 and 1,668 cm^{-1}. The band at 1,668 cm^{-1} and those at 1270 and 1326 cm^{-1} are attributed to amide I and amide III stretching modes, and those at 958 and 1070 cm^{-1} are attributed to phosphate and carbonate hydroxyapatite, respectively. The band at 862 cm^{-1} may be attributed to the vibration bands of C–C and C–C–H stretch of collagen and lipid. The band at 1,447 cm^{-1} is attributed to the bending and stretching modes of CH groups of lipids and proteins [27, 28, 30, 37].

Our team has used Raman spectroscopy to study the effects of both laser therapy and LPT on bone healing in animal models. Our previous results show that the use of near-infrared LPT is effective in improving bone repair. It seems that its higher penetration into bone is one of the factors involved. The use of LPT in studies involving bone healing is a striking topic these days, and many previous studies have demonstrated positive results, including when the light is combined with biomaterials and GBR [8, 21–37]. We have found strong evidence that the improvement in the maturation of irradiated bone is associated with an increased deposition of calcium hydroxyapatite (CHA) during the early stages of healing. This maturation may be a result of an increased secretion by osteoblasts in irradiated subjects. It is well accepted that deposition of CHA represents bone maturation, larger amounts of CHA on bone being indicative of a more resistant and calcified bone [8, 21–37].

Although several reports have suggested benefits of the individual and combined use of MTA, GBR and LEDs on wound healing, the combined use of all these techniques has not yet been studied by Raman spectroscopy.

Material and methods

The Animal Ethics Committee of Vale do Paraíba University (UNIVAP) approved this research. Ninety healthy adult male Wistar rats (about 2 months old, mean weight 295±25 g) were kept under natural conditions of light, humidity and temperature in the animal house of the Research and Development Institute of UNIVAP during the experimental period. The animals were fed with standard laboratory pelleted diet and had access to water ad libitum. The animals were kept in groups of five in individual metal cages, and kept under a day/night light cycle and controlled temperature conditions during the experimental period. The animals were randomly distributed into ten groups each of which was then subdivided into three subgroups according to the experimental schedule. The treatment groups are shown in Table 1.

Prior to induction of general anesthesia, the animals received 0.04 ml/100 g of atropine subcutaneously. Anesthesia was induced by intramuscular injection of 10% quetamine (Syntec do Brasil, Cotia, SP, Brazil; 0.1 ml/100 g)+2% xylazine (Syntec do Brasil; 0.1 ml/100 g). The right leg of the animals was shaved and a 3-cm incision was made over the right tibia with a no. 15 scalpel blade. Skin and subcutaneous tissues were dissected down to the periosteum, which was gently sectioned to expose the bone. A 2-mm partial thickness bone defect was surgically produced (low-speed drill, 1,200 rpm, under refrigeration) in each animal.

Table 1 Treatment groups

Group	Treatment
1	Blood clot
2	MTA
3	MTA+GBR
4	MTA+BMP
5	MTA+BMP+GBR
6	Blood clot + LED
7	MTA+LED
8	MTA+GBR+LED
9	MTA+BMP+LED
10	MTA+BMP+GBR+LED

The bone defects in groups 1 and 6 were filled only with blood clot. Animals in group 6 were further irradiated with LED light. The bone defects in the animals in the remaining groups were filled with MTA (Angelus; Angelus Indústria de Produtos Odontológicos, Londrina, PR, Brazil) and collagen gel (Gencol; Baumer, Mogi das Cruzes, São Paulo, Brazil). The animals in group 7 were further irradiated with LED light. In groups 3 and 8, the defects filled with the MTA were covered with a reabsorbable membrane (Genderm; Baumer). Animals in group 8 were further irradiated with LED light. In groups 4, 5, 9 and 10 a pool of BMPs (Genpro; Baumer) was added to the MTA. In group 5 the defects were covered with membrane. In group 9 the animals were further irradiated with LED light, and in group 10 the animals were further irradiated with LED light after the defects had been covered with membrane. All wounds were routinely sutured and the animals received a single dose of Pentabiotico (penicillin, streptomycin, 20,000 IU; Fort Dodge, Campinas, SP, Brazil; 0.02 ml/100 g) immediately after surgery. Animals were killed on days 15, 21 and 30 after surgery with an overdose of general anesthetics.

LPT was carried out using a FisioLED device (MMOptics, São Carlos, São Paulo, Brazil) with a wavelength of 850±10 nm, a power of 150 mW, a spot size of about 0.5 cm^2, and an energy density of 16 J/cm^2. The LED was applied transcutaneously over the defect immediately after surgery and then at 48-h intervals over 15 days resulting in a total treatment dose of 112 J/cm^2. The doses were based

upon previous studies carried out by our group using laser light [8, 21–37].

After the animals were killed, samples were longitudinally cut under refrigeration using a precision saw (IsoMet 1000; Buehler, Markham, Ontario, Canada) and stored in liquid nitrogen to minimize the growth of aerobic bacteria [27, 28, 30, 37] and because chemical fixation is not advisable due to fluorescence emissions from fixative substances [27, 28, 30, 37].

Prior to the Raman study, the samples were longitudinally cut and warmed gradually to room temperature, and 100 ml of saline was added to the surface during spectroscopic measurements. For Raman measurements, an Ti:sapphire laser with a wavelength of 830 nm pumped with an argon laser (model 3900S; Spectra Physics, Mountain View, CA) provided near-infrared excitation. A spectrograph (model 250 IS; Bruker Optics, Billerica, MA) with a spectral resolution of about 8 cm^{-1} dispersed the Raman-scattered light from the sample and a liquid nitrogen-cooled deep depletion charge-coupled device (model LN/CCD-1024-EHR1; Princeton Instruments, Tucson, AZ) was used to detect the Raman spectra. The system was controlled by a microcomputer, which stored and processed the data [27, 28, 30, 37]. The laser power used at the sample site was of 80 mW with a spectral acquisition time of 100 s. Two points were measured in transverse sections of healing bone resulting in two readings from each specimen and 180 total spectra. All spectra were acquired on the same day to avoid optical misalignments and changes in laser power. The mean values of the intensity of the peaks (about 958 cm^{-1} for phosphate ν_1, and at about 1,447 cm^{-1} for CH groups of lipids and proteins ν_2) were determined as the average of the peaks in these regions. This intensities are related to the concentration of CHA and organic components of the bone. The data were analyzed using MatLab5.1 software (Newark, NJ) for calibration and background subtraction of the spectra.

For calibration, the Raman spectrum of the solvent indene with known peaks was used [27, 28, 30, 37] due to its intense bands (800–1,800 cm^{-1}) in the fingerprint region. The indene spectrum was also measured each time the sample was changed to be sure that the laser and collection optics were optimized. In order to remove the fluorescence background from the original spectrum, a 5th order polynomial fitting was found to give better results, facilitating the visualization of the peaks of CHA (about 958 cm^{-1}) and CH groups of lipids and proteins (about 1,447 cm^{-1}) found in the bone (Fig. 1). This routine removed any continuous offset background noise due to CCD readout and refrigeration.

Statistical analysis was performed using Minitab 15.0 software (Minitab, Belo Horizonte, MG, Brazil). A baseline Raman spectrum of nontreated bone was also produced as a control. Raman analysis was carried out at the Biomolecular Spectroscopy Laboratory at the Research and Development Institute of UNIVAP.

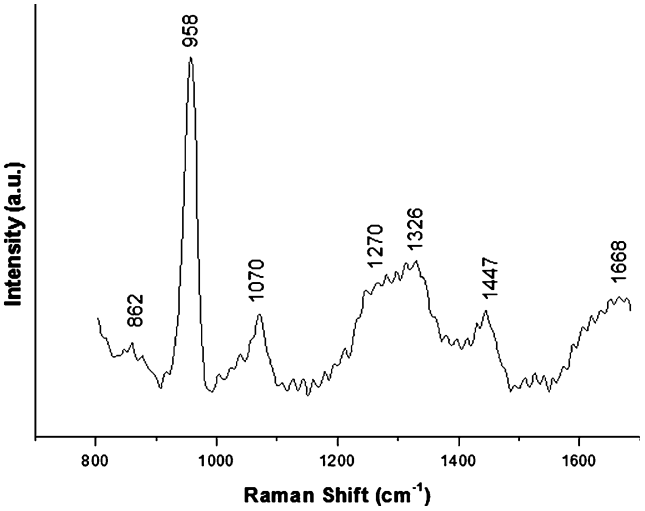

Fig. 1 Typical Raman spectrum of the components bone showing the two Raman shifts used as markers in this study (CHA at 958 cm^{-1}, CH vibration mode of lipids and proteins at 1,447 cm^{-1})

Results

The Raman spectrum of bone shows prominent vibrational bands related to tissue composition (mineral and organic matrices). Figure 1 shows the main tissue Raman bands at 862, 958, 1,070, 1,270, 1,326, 1,447 and 1,668 cm^{-1}. The band at 1,668 cm^{-1} and those at 1,270 and 1,326 cm^{-1} are attributed to amide I and III stretching modes of lipids and proteins. The band at 1,447 cm^{-1} is attributed to the bending and stretching vibration modes of CH groups of lipids and proteins. The bands at 958 and 1,070 cm^{-1} are attributed to phosphate and carbonate hydroxyapatite from bone mineral, respectively, and that at 862 cm^{-1} may be attributed to the vibration bands of C–C stretch of collagen (tyrosine/proline ring).

Hydroxyapatite (CHA, 958 cm^{-1})

Figures 2, 3, 4, 5 and 6 show respectively the values of the mean intensity of each Raman shift of CHA (958 cm^{-1}) and the organic components of bone (CH vibration groups of lipids and proteins, 1,447 cm^{-1}) obtained from treated and untreated animals on days 15, 21 and 30. The intensity of the Raman shift is directly related to the concentration/incorporation of CHA by the bone. So higher intensities represent higher concentrations of CHA. It should be noted that in some groups, irradiated or not, the initial value of the peak was higher than on day 21. This might have been

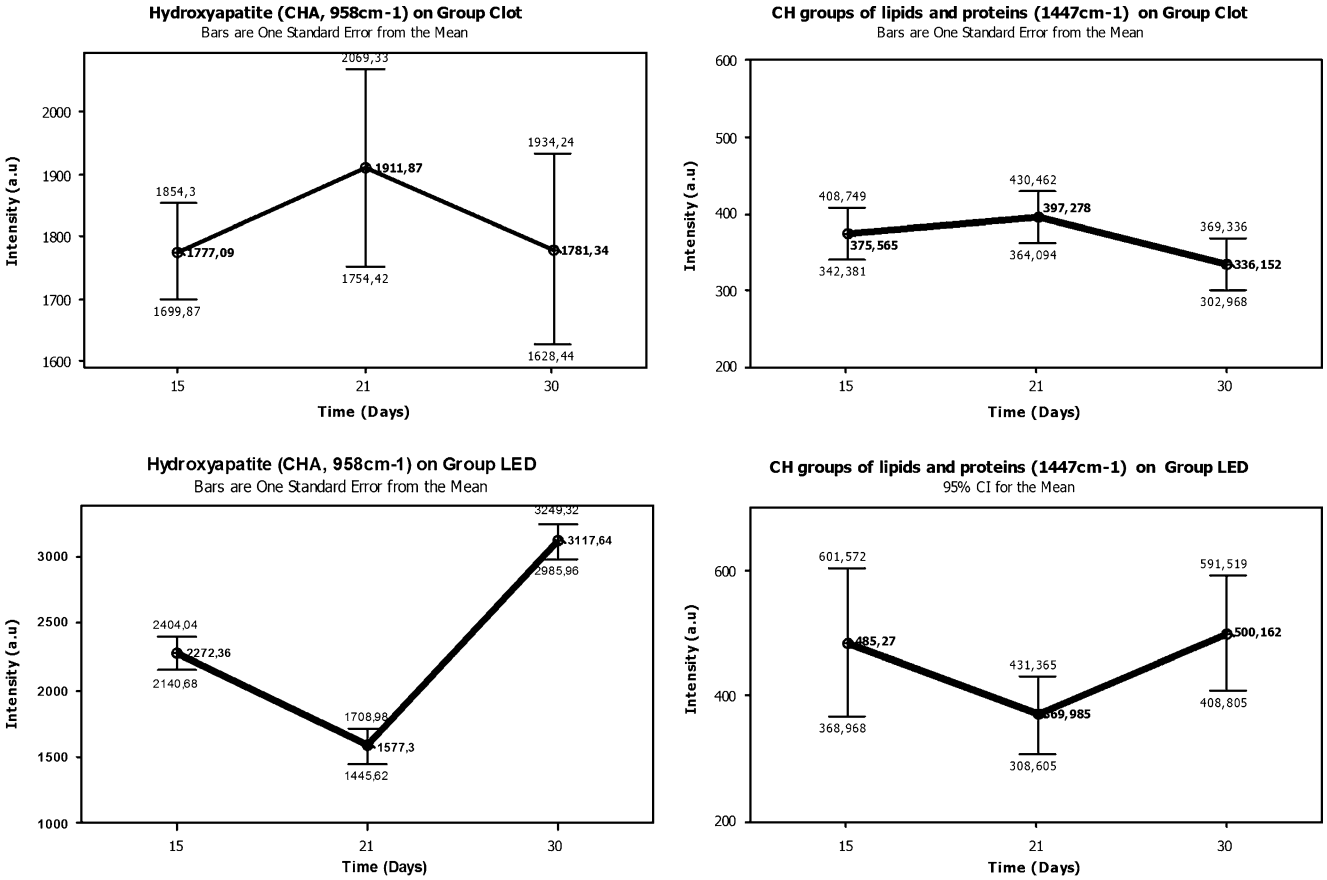

Fig. 2 Mean intensities of the Raman shifts of CHA (958 cm^{-1}) and CH vibration groups of lipids and protein (1,447 cm^{-1}) in group 1 (*Clot*) and group 6 (*LED*) on days 15, 21 and 30

caused by the characteristics of the MTA present at the site. Table 2 shows a summary of the statistical analysis at each time-point.

There were no statistically significant differences in the CHA peaks among the nonirradiated groups at all experimental time-points. On the other hand, there were statistically significant differences between group 1 and the irradiated groups at all time-points (ANOVA, $p<0.001$, $p=0.02$, $p<0.001$). On day 15, group 9 showed a higher mean peak value (3,042.9±209) and group a lower value (1,475.5±106). On day 21 group 9 also showed a higher mean peak value (2,371±778) and group 10 a lower mean peak value (1,404.2±71). At the end of the experimental period, group 6 showed the highest mean peak value (3,117.6±100) and group 10 the lowest (1,386±140).

There was a statistically significant difference between the mean CHA peak in nonirradiated groups at all the experimental time-points (ANOVA, $p<0.01$). The mean peak value in group 1 was significantly different from that in group 2 (Student's *t*-test, $p<0.001$). A statistically significant difference was seen between group 1 and the irradiated groups (ANOVA, $p<0.001$). Table 3 shows a summary of the statistical analysis for each treatment group.

CH vibration groups of lipids and proteins (1,447 cm^{-1})

The results for the organic components of bone (CH vibration groups of lipids and proteins, 1,447 cm^{-1}) are shown in Table 4 and Figs. 2, 3, 4, 5 and 6. Higher peaks indicate a lower mineral content and higher readings denote higher levels of organic components.

The analysis of the CH peaks showed statistically significant differences among the nonirradiated groups on day 15 (ANOVA, $p=0.007$). Group 1 showed the highest mean peak value (375.6±35) and group 3 the lowest (270.28±28). Despite no statistically significant difference being observed on day 21, at the end of the experimental period, a statistically significant difference was observed among the nonirradiated groups (ANOVA, $p=0.003$) the highest mean peak value being seen in group 4 (434.9±66) and the lowest in group 2 (304.1±40).

Among the irradiated groups, statistically significant differences were also observed at similar time-points as seen in the nonirradiated groups. On day 15, group 6 showed the highest mean peak value (485.3±111) and group 10 the lowest (314.7±52) (ANOVA, $p=0.003$). Despite no statistically significant difference being observed on day 21,

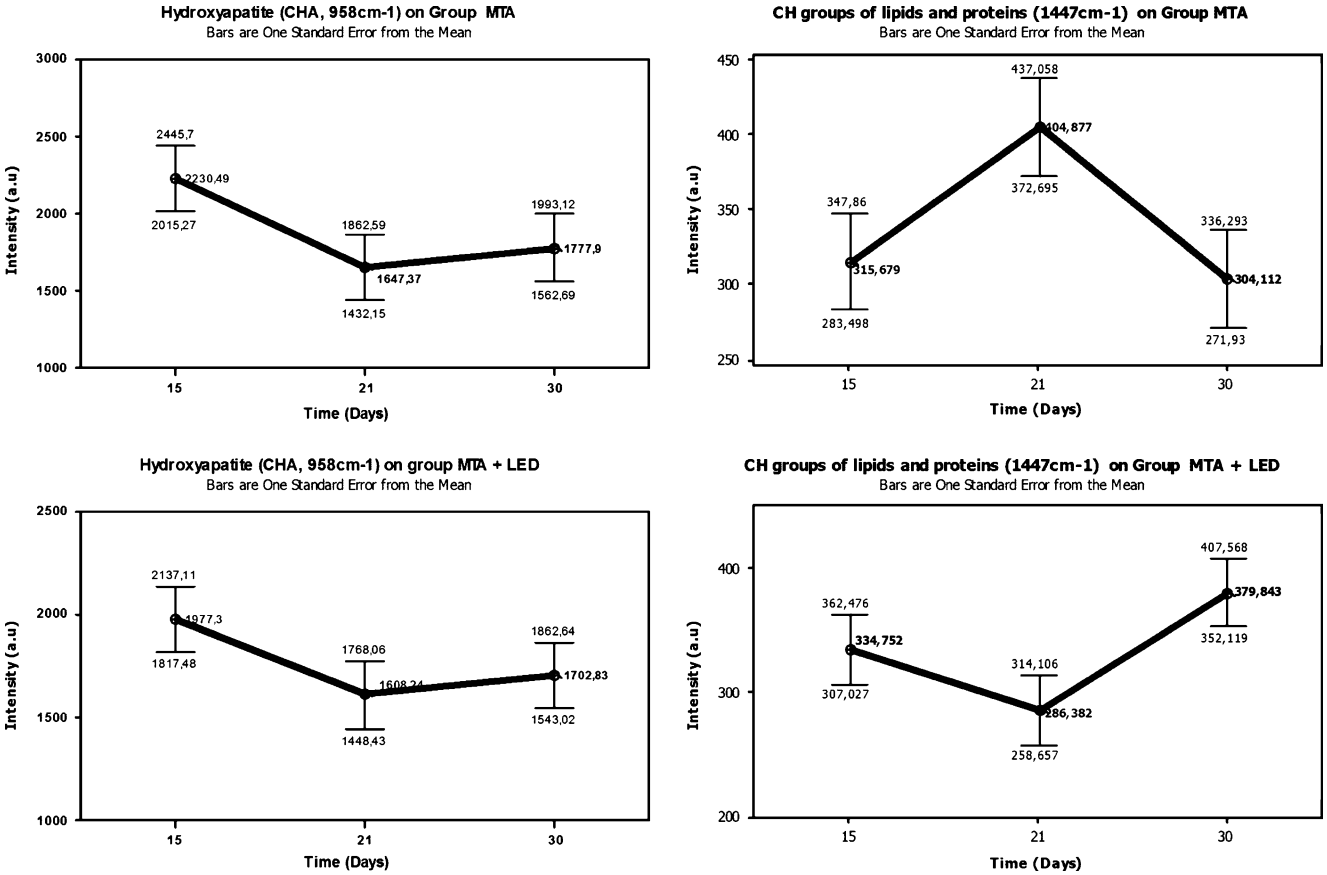

Fig. 3 Mean intensities of the Raman shifts of CHA (958 cm^{-1}) and CH vibration groups of lipids and protein (1,447 cm^{-1}) in groups 2 (*MTA*) and 7 (*MTA+LED*) on days 15, 21 and 30

there was a statistically significant difference at the end of the experimental period (ANOVA, $p=0.001$), the highest mean peak value being observed in group 6 (500.2±87) and the lowest in group 8 (313.6±44). Table 4 shows a summary of the statistical analysis at each time-point.

Statistically significant differences were seen among the nonirradiated groups at all experimental time-points (ANOVA, $p=0.05$), the highest mean peak value being seen in group 4 (374.51±73.33) and the lowest in group 3 (307.8±64). Among the irradiated groups, there was also statistically significant difference between group 1 and all the irradiated groups (ANOVA, $p<0.001$), the highest mean peak value being seen in group 6 (451.8±102) and the lowest in group 10 (317±75). Table 5 shows a summary of the statistical analysis for each treatment group.

Discussion

The Wistar rat model adopted in the present investigation shows a rapid healing period, is resistant to climatic changes and is routinely used to study bone healing. Despite LPT having been shown to improve bone healing in several models [8, 21–37], there have been few studies of the use of LED light on bone and there are no studies until now of its combination with biomaterials. Studies of the effects of laser light on bone regeneration have indicated that its effect on bone healing depends not only on the total dose of irradiation, but also on the irradiation time and the irradiation mode [8, 21–37]. We were unable to find any previous reports in the literature concerning the use of the protocol used in the present investigation. This makes discussion of our results very difficult.

Previous studies have found that irradiated bone (mostly irradiated with IR wavelengths) shows increased osteoblastic proliferation, collagen deposition and bone neoformation when compared to nonirradiated bone. The protocol used in the present study using LED light is similar to those used by our team in previous studies using laser light [8, 21–36]. The results of the present study are promising and indicate that the combination of LED light and MTA, BMPs and GBR did improve the healing of bone.

Our team has been studying the effects of different light sources on bone healing using different assessment methods including histology, computerized morphometry, scanning electron microscopy and Raman spectroscopy [8,

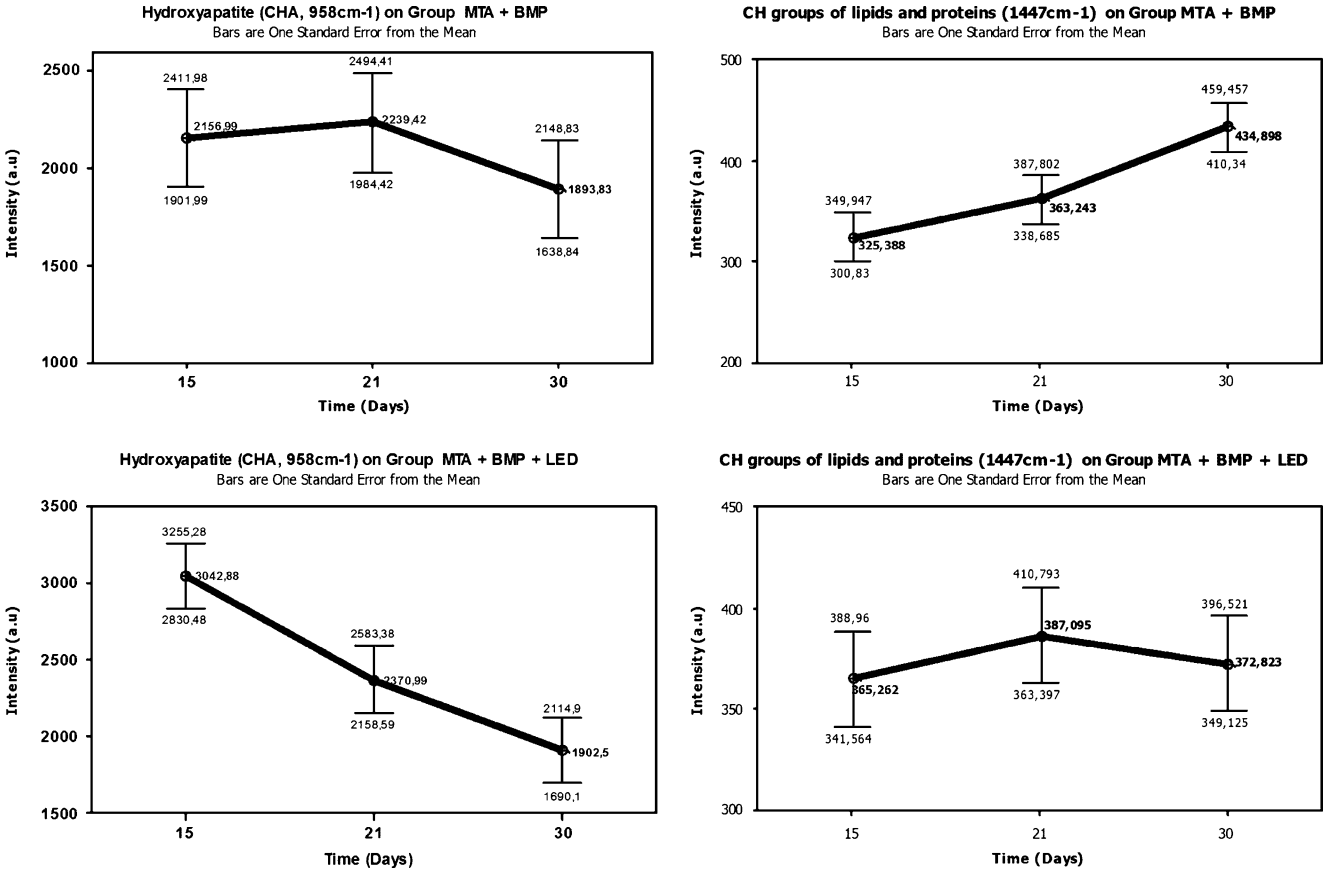

Fig. 4 Mean intensities of the Raman shifts of CHA (958 cm^{-1}) and CH vibration groups of lipids and protein (1,447 cm^{-1}) in group 4 (*MTA+ BMP*) and group 9 (*MTA+ BMP+ LED*) on days 15, 21 and 30

21–37]. Raman spectroscopy was used in the present study to analyze alterations in both mineral and organic components in healing bone as analysis of bone components is considered the gold standard in the study of bone healing [27, 28, 30, 37].

Raman spectra are a plot of the scattering intensity as a function of the energy difference between the incident and scattered photons and are obtained by pointing a monochromatic laser beam at a sample. The loss (or gain) in photon energy corresponds to the difference in the final and initial vibrational energy levels of the molecules participating in the interaction. The resultant spectra are characterized by shifts in wave numbers (inverse of wavelength in cm^{-1}) from the incident frequency. The frequency difference between incident and Raman-scattered light is termed the Raman shift, which is unique for individual molecules and is measured by the machines detector and is represented as 1/cm. Raman peaks are spectrally narrow, and in many cases can be associated with the vibration of a particular chemical bond (or a single functional group) in the molecule [38].

A number of researchers have reported on Raman spectroscopy of biological tissues, which include investigations on bone, cornea, cervical tissue, epithelial tissue, lung, breast, skin, gastrointestinal tissue, brain, oral tissue, liver, heme protein, atherosclerotic plaque, serum, human coronary arteries, lymphocytes, human red blood cells, mixed cancer cells, living human cells, microbial cells, individual cells, saliva, DNA, cancer genes, anticancer drugs, tissue processing, raft cultures, meningioma, cancerous cells, and mammalian cell cultures [38].

Our results indicate that infrared LED light causes a quicker repair process and improves the quality of the newly formed bone as marked by the CHA peaks. These findings are aligned with those of previous studies using laser light carried out by our team using several models [8, 21–37]. Our experience indicates that the advanced maturation seen in irradiated bone is due to an increased deposition of CHA. The enhancement in maturation represents the ability of irradiated osteoblasts to secrete more CHA. Increased amounts of CHA are indicative of bone maturation as well as of more resistant and calcified bone. We have also shown that infrared laser light is able to stimulate proliferation of fibroblasts which are major secretors of collagen and an important organic component on healing bone [8, 21–37]. The Raman spectroscopy results in the present investigation

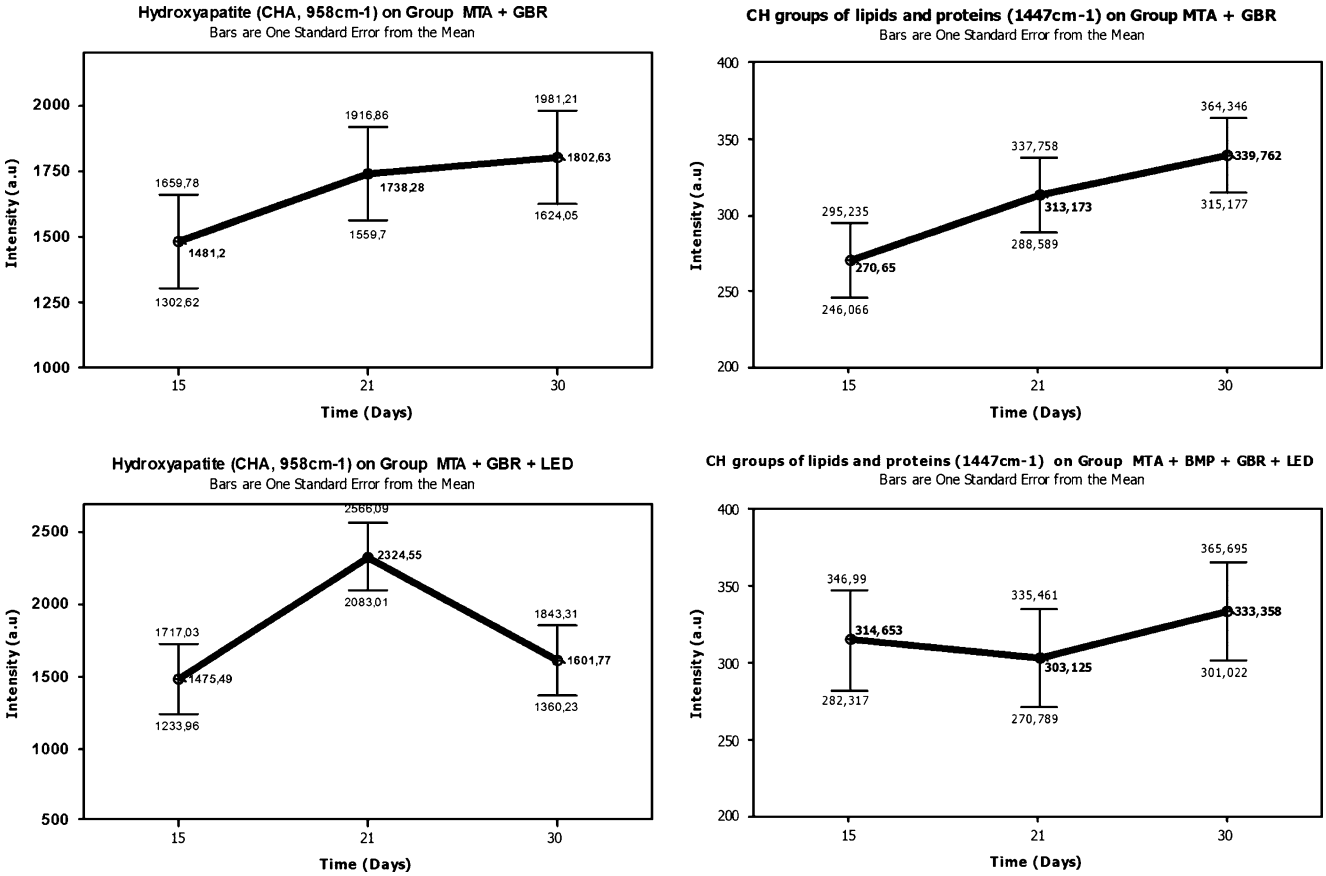

Fig. 5 Mean intensities of the Raman shifts of CHA (958 cm^{-1}) and CH vibration groups of lipids and protein (1,447 cm^{-1}) in group 3 (*MTA+GBR*) and group 8 (*MTA+GBR+LED*) on days 15, 21 and 30

indicate the occurrence of such phenomena when LED light is used.

MTA appeared to be directly affected by the light. However, LPT positively affected bone healing as has been observed in other studies using other biomaterials and laser light [8, 21–36]. In the early stages of the bone repair, a higher mean CHA peak was seen in group 9 (MTA+BMP+LED) and at the end of the experimental period, and the highest mean peak was seen in group 6 (LED). We were not able to find in the literature any previous reports on the association between MTA and BMPs. However, the use of BMPs improves the outcome of bone healing when associated with LPT [23–25, 36, 37]. In the present study, this was the case up to day 21. Later, the use of LED light alone caused the greatest increase in the levels of CHA. However, analyzing all the changes throughout the experimental period, group 9 (MTA+BMP+LED) showed the higher mean CHA peak.

The behavior of the lipids and proteins varied greatly throughout the experimental period in most groups. This may indicate that other tissue components might have affected the readings. Although we were able to show differences in the peaks of lipids and proteins, LED-irradiated bones showed a higher collagen content at early stages of repair, this possibly being associated with increased collagen deposition by fibroblasts that were stimulated by the LED light, similar to the observations when using laser light [27, 28, 30, 36, 37]. On the other hand, at the end of the experimental period, group 8 (MTA+GBR+LED) showed lower mean peaks. This may also represent the influence of the use of the GBR. The reason for this needs clarification. The overall content of lipids and proteins analyzed during the whole experimental period showed that the association of MTA+BMP+GBR+LED was associated with lower amounts of these components compared to all irradiated groups. However, the levels of lipids and proteins in this group was similar to the levels seen in group 2 (MTA), that showed the smallest peak. This was probably due to the properties of the MTA itself.

It has also been demonstrated by our group that the use of GBR is helpful in the healing of bone defects and that combining it with LPT improves the outcome of this therapeutic approach as demonstrated previously by our team using different models [8, 22–25, 27, 29, 31, 33]. However, its combination with MTA and/or LED light seemed not to have major influence. Probably, this was due

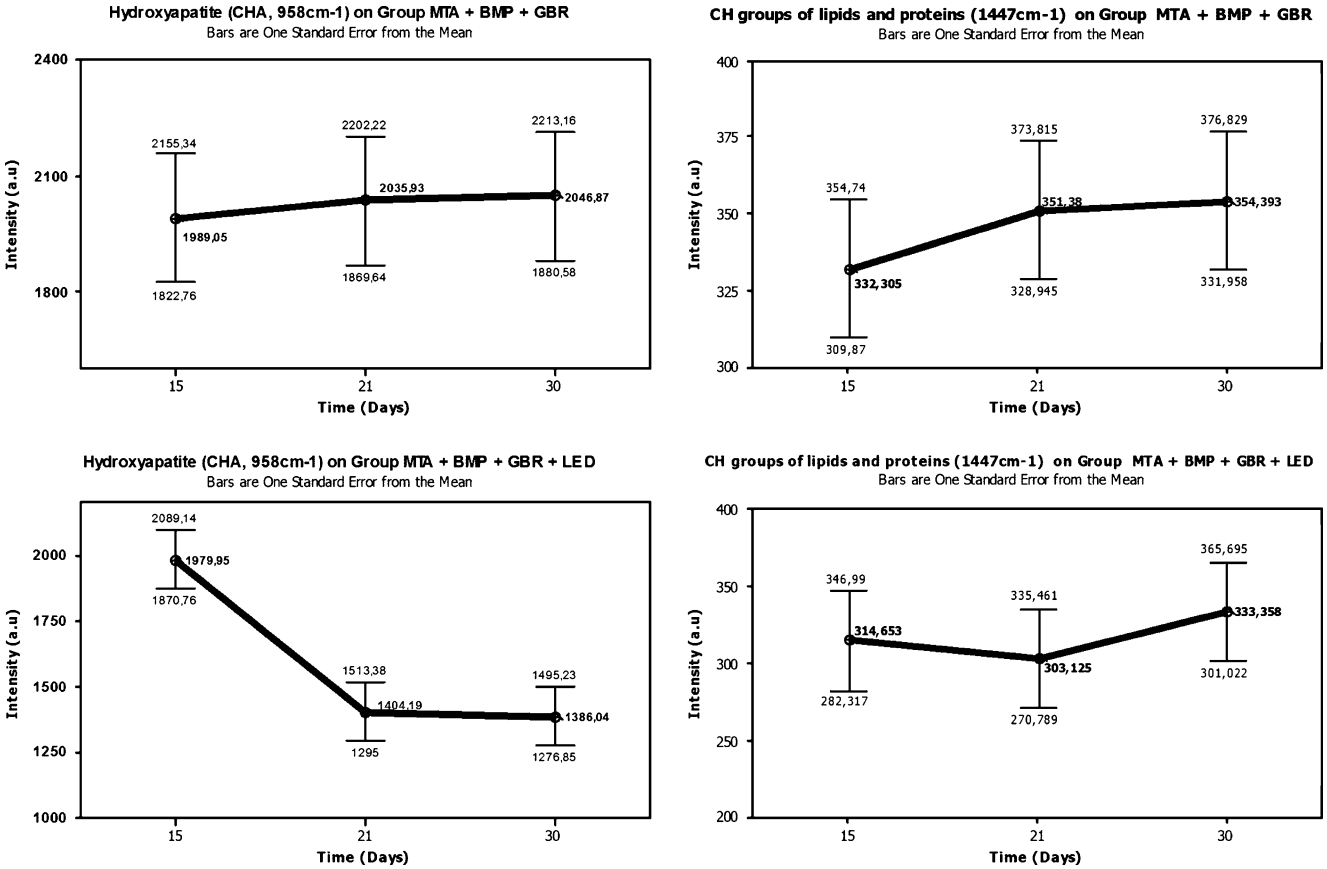

Fig. 6 Mean intensities of the Raman shifts of CHA (958 cm^{-1}) and CH vibration groups of lipids and protein (1,447 cm^{-1}) in group 5 (*MTA + BMP + GBR*) and group 10 (*MTA + BMP + GBR + LED*) on days 15, 21 and 30

to the relative stiffness of the MTA graft that in some way may have acted as a barrier against invasion by the tissue. Another aspect that might have influenced the results observed in the LED-irradiated groups in which the GBR was used was the fact that the LED irradiation was carried out over the defect at a single point, differently from situations in which Laser light is used as many devices have a very small spot size. In the present study, the LED device used had a relatively wide spot and probably the membrane acted as an attenuation barrier for light penetration.

One may question why the use of BMPs alone was not assessed on the present study. First, it is important to note that the use of BMPs alone is still complicated as their life-span in this situation is very short. So the use of some matrices, organic or inorganic, will delay the otherwise rapid dispersion of water-soluble, readily diffusible BMPs

Table 2 Values (means ± standard deviation) of the Raman peak for CHA (958 cm^{-1}) in all the treatment groups on days 15, 21 and 30

Group	Treatment	Group letter	Day 15	Day 21	Day 30
1	Blood clot	a	$1,777.1\pm189.1^{f,g,i}$	$1,912\pm157^{f,i,j}$	$1,691\pm303^{f,i,j}$
2	MTA	b	2,230±677	1,647±508	1,778±343
3	MTA+GBR	c	1,481±420	1,738±490	1,803±396
4	MTA+BMP	d	2,157±715	2,239±639	1,894±501
5	MTA+BMP+GBR	e	1,989±368	2,035.9±227	2,047±557
6	LED	f	$2,272\pm279^{a,h}$	$1,577\pm474^{a}$	$3,117.6\pm100^{a,g,h,i,j}$
7	MTA+LED	g	$1,977\pm646^{a,i}$	1,608.2±187	$1,702.8\pm89^{f,j}$
8	MTA+GBR+LED	h	$1,475.5\pm106^{f,i,j}$	2,325±996	$1,601.8\pm214^{f}$
9	MTA+BMP+LED	i	$3,042.9\pm209^{a,g,h,i}$	$2,371\pm778^{a}$	$1,903\pm403^{a,f,j}$
10	MTA+BMP+GBR+LED	j	$1,980\pm436^{h,i}$	$1,404.2\pm71^{a}$	$1,386\pm140^{a,f,g,i}$

Superscript letters indicate that the value is significantly different from the value of the group with the same letter

Table 3 Values (means ± standard deviation) of the Raman peak for CHA (958 cm^{-1}) in all the treatment groups

Group	Treatment	Group letter	Mean ± SD
1	Blood clot	a	$1{,}823.4\pm316^{b,i,j}$
2	MTA	b	$1{,}885\pm558^{a}$
3	MTA+GBR	c	$1{,}674\pm435^{d,e,j}$
4	MTA+BMP	d	$2{,}096\pm606^{c,i}$
5	MTA+BMP+GBR	e	$2{,}024\pm383^{c,j}$
6	LED	f	$2{,}322.4\pm715^{g,j}$
7	MTA+LED	g	$1{,}762.8\pm401^{f,i}$
8	MTA+GBR+LED	h	$1{,}800.6\pm676^{i}$
9	MTA+BMP+LED	i	$2{,}438.8\pm686^{a,d,g,h,j}$
10	MTA+BMP+GBR+LED	j	$1{,}590.1\pm379^{a,c,e,f,i}$

Superscript letters indicate that the value is significantly different from the value of the group with the same letter

from the implant site without which they, like other growth factors, would likely have a short serum half-life because of liver uptake and catabolism [39–42]. On the other hand, the use of some BMPs (2 and 7) is approved for clinical use for osseous repair and are well accepted as therapeutic modalities [43, 44].

Normal bone regeneration is a complex process that involves a large number of growth factors and cytokines in its regulation. No matter how influential one factor may appear in the process, its action in isolation may have little effect without interaction with endogenously produced growth factors and cytokines [45]. Among the many tissues in the body, bone has the highest potential for regeneration. Bone morphogenesis is a sequential multistep biological chain reaction and the key steps are chemotaxis of progenitors/stem cells, proliferation of cells and differentiation of true endochondral bone formation.

The role of growth factors in bone repair is widely recognized, particularly for BMPs, fibroblast growth factor (FGF), insulin-like growth factors (IGFs), platelet-derived growth factor (PDGF), transforming growth factor-β (TGF-β) and vascular endothelial growth factor (VEGF). Growth factors are usually stored in the extracellular matrix (ECM), but after injury are actively released by the ECM, cells and platelets. The main growth factors acting on the skeleton are BMPs, TGF-β, FGF, PDGF, VEGF and IGFs. During bone repair, cells of the bone microenvironment, such as inflammatory cells, fibroblasts, endothelial cells, bone marrow stromal cells and osteoblasts produce growth factors. The migration of osteoprogenitors is enhanced by BMPs, PDGF, FGF and VEGF. The proliferation of periosteum-derived cells is stimulated by PDGF and FGF in the early stages of bone repair. Previous studies have found that light is capable of altering the release of several growth factors [46–50].

Artificial materials, such as the MTA, may influence the synthesis and release growth factors from cells. The final effect depends on both the biomaterial's physical and chemical properties and the cell involved. So, bone induction, and its subsequent regeneration, might not only be restricted to biological modulation but the environment might also be a crucial factor in the induction and subsequent regeneration of bone. There is evidence that the platelet release reaction is induced at a different level by some bone substitutes: collagen-grafted calcium metaphosphate induces a higher release reaction than nongrafted calcium metaphosphate or hydroxyapatite. These effects should be carefully considered and evaluated when a new material is proposed as a scaffold for bone engineering [51, 52]. We were unable to find a previous study assessing this aspects using MTA.

One drawback in using this material is that close proximity to the host bone was necessary to achieve osteoconduction. However, new bone growth is often strictly limited because these materials are not osteoinductive in nature. To overcome this limitation, a number of different bone-derived growth factors have been demonstrated to stimulate bone growth, collagen synthesis and fracture repair both in vitro and in vivo. MTA also suffers

Table 4 Values (means ± standard deviation) of the Raman peaks for the CH groups of lipids and proteins (1,447 cm^{-1}) in all the treatment groups on days 15, 21 and 30

Group	Treatment	Group letter	Day 15	Day 21	Day 30
1	Blood clot	a	$375.6\pm35^{c,d,f,j}$	397.3±127	$336.2\pm49^{d,f}$
2	MTA	b	315.7±52	404.9±120	$304.1\pm40^{c,d,e}$
3	MTA+GBR	c	$270.7\pm28^{a,d}$	313.2±87	$339.8\pm50^{b,d,e}$
4	MTA+BMP	d	$325.4\pm38^{a,c}$	363.2±71	$434.9\pm66^{a,b,c,e}$
5	MTA+BMP+GBR	e	332.3±57	351.4±53	$354.4\pm54^{b,c,d}$
6	LED	f	$485.3\pm111^{a,g,h,i,j}$	370±58	$500.2\pm87^{a,g,h,i}$
7	MTA+LED	g	334.8 ± 78^{f}	286.4±70	$379.8\pm54^{f,j,h}$
8	MTA+GBR+LED	h	343.9 ± 74^{f}	321.2±104	$313.6\pm44^{f,i,g}$
9	MTA+BMP+LED	i	365.3 ± 35^{f}	387.1±75	$372.8\pm57^{f,h}$
10	MTA+BMP+GBR+LED	j	$314.7\pm52^{a,f}$	303.1±72	333.4 ± 105^{g}

Superscript letters indicate that the value is significantly different from the value of the group with the same letter

Table 5 Values (means ± standard deviation) of the Raman peak for the CH groups of lipids and proteins (1,447 cm^{-1}) in all the treatment groups

Group	Treatment	Group letter	Mean ± SD
1	Blood clot	a	$369.6\pm81^{c,f}$
2	MTA	b	341.5 ± 87
3	MTA+GBR	c	$307.8\pm64^{a,d,e}$
4	MTA+BMP	d	374.5 ± 73^{c}
5	MTA+BMP+GBR	e	346 ± 52^{c}
6	LED	f	$451.8\pm102^{a,g,h,i,j}$
7	MTA+LED	g	$333.6\pm75^{f,i}$
8	MTA+GBR+LED	h	$326.2\pm74^{f,i}$
9	MTA+BMP+LED	i	$375\pm55^{f,g,h,j}$
10	MTA+BMP+GBR+LED	j	$317\pm75^{f,i}$

Superscript letters indicate that the value is significantly different from the value of the group with the same letter

from its inherent lack of microporosity for tissue invasion. Its pore size and inherent strength play major roles in its ultimate usefulness. Previously it was generally believed that calcium phosphate cements are reabsorbed with bone formed via osteoconduction. However, recent studies have indicated that calcium phosphate cements directly initiate osteogenesis. In addition, through a dissolution–precipitation process, the development of a bone-like mineral layer might initiate bone formation either by mimicry with the bone mineral structure or by the presence of osteogenic compounds (such as BMPs) [53, 54].

BMPs have been defined as a molecule (morphogen) that can initiate, promote and maintain metabolism and homeostasis [55]. However, the mere presence of BMPs is no guarantee of efficient bone healing. Although the presence of BMPs is essential for a number of processes during bone healing, BMP-mediated bone formation strongly depends on the local presence of various BMP activity regulating inhibitors and stimulators. The osteogenic potency of the BMPs requires a local and controlled delivery. Moreover, for clinical use of BMPs, their short half-life should be taken into account [56]. BMPs were initially discovered by the fact that demineralized bone matrix is capable of initiating bone formation when transplanted to ectopic sites in rodents [57]. These proteins were originally described to act as bone growth factors. The BMP family of cytokines comprises over 20 different ligands that belong to the TGF-β superfamily. Their importance in the development of multicellular organisms is obvious from their existence in all vertebrates as well as nonvertebrate animals [45]. Although BMPs are involved in numerous developmental and pathophysiological processes, their effects on bone formation have been studied most extensively. In bone, they are synthesized by skeletal cells such as osteoblasts and sequestered in the bone ECM [45].

It is known that when BMPs are implanted, their osteoinductive properties can initiate the complete cascade of bone formation, including the migration of mesenchymal stem cells and their differentiation into osteoblasts. This bone induction occurs through endochondral as well as intramembranous ossification and results in the formation of normal woven and/or lamellar bone [58]. Various proteins with an important role in this autoinductive process have been isolated and investigated for their therapeutic potential in bone regeneration, including BMPs [59], TGF-β, FGF, IGF, VEGF, PDGF, epidermal growth factor, parathyroid hormone/parathyroid hormone-related protein and interleukins [45].

The production of growth factors is a biological process that starts immediately after injury and stimulates the cells involved in the repair process to proliferate. TGF-β is a multifunctional cytokine secreted by platelets, T lymphocytes, macrophages, endothelial cells, fibroblasts and other tissues. It has a central action and has antiinflammatory and proliferative effects during tissue repair. Its effects include chemotaxis of leukocytes, fibroblasts and smooth muscle cells. It also influences both the formation and remodeling of the ECM, stimulates keratinocyte migration, and angiogenesis and fibroblastic differentiation, inhibits the proliferation of keratinocytes, regulates the expression of integrin and other cytokines, and also possesses an autoinduction property [46].

TGF-β is synthesized by many different cell types and is stored as an inactive complex with latency-associated peptide in the bone ECM. Another major source of this factor is platelets in the blood clot formed after a fracture or the creation of a bone defect. It is known that TGF-β stimulates migration of osteoprogenitor cells and is a potent regulator of cell proliferation, cell differentiation and ECM synthesis, and that it synergizes with BMPs. Early during repair, both growth factors may directly increase the number of osteoprogenitor cells by stimulating their migration. Circulation is one of the sources of osteoprogenitor cells during BMP-induced bone regeneration and cell recruitment may also be indirectly enhanced by their combined effect on angiogenesis. It has been suggested that TGF-β1 and BMP-7 synergistically interact to enhance angiogenesis and vascular invasion since their coadministration increases vessel formation. The mitogenic effect of TGF-β may further increase the osteoprogenitor cell pool by stimulating cell proliferation [45]. As well as their combined effects on angiogenesis, cell recruitment and proliferation, TGF-β and BMPs also interact during osteoblast differentiation [60]. Light has also been shown to increase angiogenesis and to increase the number and activity of osteoblasts [8, 22–26, 29, 31–33, 35].

It has been suggested that TGF-β1 may have stimulatory effects on osteoblast differentiation during early stages and an inhibitory effect on differentiation and mineralization

during later stages. Although TGF-β1 seems to inhibit matrix mineralization during later stages, the in vivo consequences of these inhibitory effects might be limited since expression of TGF-β receptors is downregulated when cell differentiation progresses [45]. This aspect is important as it may be one explanation for our previous results indicating that infrared light fails to significantly enhance bone repair during the later stages [8, 22–37]. A pivotal role in the bone remodeling process has been assigned to TGF-β1 because it has been proven to affect both bone resorption and formation. It is secreted in a latent form by bone cells and is stored in the ECM. Active resorbing osteoclasts are capable of activating TGF-β1, which in turn attenuates further bone resorption by impairing osteoclastogenesis and promotes bone formation through chemotactic attraction and stimulation of proliferation and differentiation of osteoblast precursors [60]. There is also evidence in the literature suggesting that light positively affects the release of TGF-β [46].

It seems possible that LED light has beneficial effects similar to those of laser light, as there are several reports of the benefits of the use of LEDs operating at several wavelengths both in vitro and in vivo in both normal and pathological conditions [2, 61–64]. It is also possible that the mechanism involved are similar.

The rationale for combining MTA, BMPs and LED light in this work was based on the idea that BMPs combined with an osteoconductive substance, such as MTA, and LED light (with its well-recognized positive effects on cell proliferation and function as well as on secretion of many growth factors) would improve the repair of bone defects in a manner similar to that following autogenous bone grafting while avoiding the complications and limitations associated with autogenous bone grafting, that remains the gold standard for treating bone defects.

Despite the success we have observed using different light sources in bone repair using different models, our knowledge of the bone regeneration process and light interactions is still limited. Therefore, further molecular, cellular, and translational studies are required to obtain a better understanding of the actions and interactions of the different regulators of the regeneration process. Our results using Raman spectral analysis indicate that infrared LED light did improve the deposition of CHA in the healing bone grafted or not with MTA.

Acknowledgments We would like to thank the Conselho Nacional de Desenvolvimento Científico e Tecnológico (CNPq) for providing financial support for this project.

Conflicts of interest The authors received a grant from the Conselho Nacional de Desenvolvimento Científico e Tecnológico (CNPq), a government research agency, but have full control of all primary data and agree to allow the journal to review their data if requested.

References

1. Barolet D (2008) Light-emitting diodes (LEDs) in dermatology. Semin Cutan Med Surg 27:227–238
2. Recker RR (1992) Embryology, anatomy, and microstructure of bone. In: Coe FL, Favus MJ (eds) Disorders of bone and mineral metabolism. Raven, New York, pp 219–240
3. Muschler GF, Lane JM, Dawson EG (1990) The biology of spinal fusion. In: Cotler JM, Cotler HB (eds) Spinal fusion: science and technique. Springer, Berlin, pp 9–21
4. Prolo DJ (1990) Biology of bone fusion. Clin Neurosurg 36:135–146
5. Kalfas IH (2001) Principles of bone healing. Neurosurg Focus 10:E1
6. Evans GH, Yukna RA, Cambre KM, Gardiner DL (1997) Clinical regeneration with guided tissue barriers: an analysis of the current literature. Curr Opin Periodontol 4:75–81
7. Nascimento C, Issa JPM, Oliveira RR, Lyomasa MM, Siéssere S, Regalo SCH (2007) Biomateriales con aplicación en el proceso de reparación óssea. Int J Morphol 25:839–846
8. Pinheiro AL, Gerbi ME (2006) Photoengineering of bone repair processes. Photomed Laser Surg 24:169–178
9. Torabinejad M, Hong CU, Lee SJ, Monsef M, Pitt Ford TR (1995) Investigation of mineral trioxide aggregate for root end filling in dogs. J Endod 21:603–608
10. Torabinejad M, Hong CU, Pitt Ford TR (1995) Physical properties of a new root end filling material. J Endod 21:349–353
11. Torabinejad M, Chivian N (1999) Clinical applications of mineral trioxide aggregate. J Endod 25:197–205
12. Schwartz RS, Mauger M, Clement DJ, Walker WA (1990) Mineral trioxide aggregate: a new material for endodontics. J Am Dent Assoc 130:967–975
13. Bystrom A, Claesson R, Sundqvist G (1985) The antibacterial effect of camphorated paramonochlorophenol, camphorated phenol and calcium hydroxide in the treatment of infected root canals. Endod Dent Traumatol 1:170–175
14. Mitchell PJ, Pitt Ford TR, Torabinejad M, McDonald F (1999) Osteoblast biocompatibility of mineral trioxide aggregate. Biomaterials 20:167–173
15. Park YJ (2000) Enhanced guided bone regeneration by controlled tetracycline release from poly(L-lactide) barrier membranes. J Biomed Mater Res 51:391–397
16. Whelan HT, Buchmann EV, Whelan NT et al (2001) NASA light emitting diode medical applications: from deep space to deep sea. Space Technol Appl Int Forum 552:35–45
17. Whelan HT, Connely MD, Hodgson BD et al (2002) NASA light emitting diodes for the prevention of oral mucositis in pediatric bone marrow transplant patients. J Clin Laser Med Surg 20:319–324
18. Al-Watban FA, Andres BL (2003) Polychromatic LED therapy in burn healing of non-diabetic and diabetic rats. J Clin Laser Med Surg 21:249–258
19. Corazza AV, Jorge J, Kurachi C, Bagnato VS (2007) Photobiomodulation on the angiogenesis of skin wounds in rats using different light sources. Photomed Laser Surg 25:102–106
20. Al-Watban FA (1997) Laser acceleration of open skin wound closure in rats and its dosimetric dependence. Lasers Life Sci 7:237–247
21. Smith KC (2005) Laser (and LED) therapy is phototherapy. Photomed Laser Surg 23:78–80
22. Pinheiro AL, Gerbi ME, Limeira Júnior FA et al (2009) Bone repair following bone grafting hydroxyapatite guided bone regeneration and infrared laser photobiomodulation: a histological study in a rodent model. Lasers Med Sci 24:234–240
23. Gerbi ME, Marques AM, Ramalho LM et al (2008) Infrared laser light further improves bone healing when associated with bone

morphogenic proteins: an in vivo study in a rodent model. Photomed Laser Surg 26:55–60
24. Pinheiro AL, Gerbi ME, Ponzi EA et al (2008) Infrared laser light further improves bone healing when associated with bone morphogenetic proteins and guided bone regeneration: an in vivo study in a rodent model. Photomed Laser Surg 26:167–174
25. Torres CS, Santos JN, Monteiro JS, Amorim PG, Pinheiro AL (2008) Does the use of laser photobiomodulation, bone morphogenetic proteins, and guided bone regeneration improve the outcome of autologous bone grafts? An in vivo study in a rodent model. Photomed Laser Surg 26:371–377
26. Gerbi ME, Pinheiro AL, Ramalho LM (2008) Effect of IR laser photobiomodulation on the repair of bone defects grafted with organic bovine bone. Lasers Med Sci 23:313–317
27. Lopes CB, Pacheco MT, Silveira Junior L, Duarte J, Cangussú MC, Pinheiro AL (2007) The effect of the association of NIR laser therapy BMPs, and guided bone regeneration on tibial fractures treated with wire osteosynthesis: Raman spectroscopy study. J Photochem Photobiol B 89:125–130
28. Lopes CB, Pinheiro AL, Sathaiah S, Da Silva NS, Salgado MA (2007) Infrared laser photobiomodulation (830 nm) on bone tissue around dental implants: a Raman spectroscopy and scanning electronic microscopy study in rabbits. Photomed Laser Surg 25:96–101
29. Weber JB, Pinheiro AL, Oliveira MG, Oliveira FA, Ramalho LM (2006) Laser therapy improves healing of bone defects submitted to autogenous bone graft. Photomed Laser Surg 24:38–44
30. Lopes CB, Pinheiro AL, Sathaiah S, Ramalho LM (2005) Infrared laser light reduces loading time of dental implants: a Raman spectroscopy study. Photomed Laser Surg 23:27–31
31. Gerbi ME, Pinheiro AL, Ramalho LM et al (2005) Assessment of bone repair associated with the use of organic bovine bone and membrane irradiated at 830 nm. Photomed Laser Surg 23:382–388
32. Pinheiro AL, Limeira Júnior FA, Gerbi ME et al (2003) Effect of low level laser therapy on the repair of bone defects grafted with inorganic bovine bone. Braz Dent J 14:177–181
33. Pinheiro AL, Limeira Júnior FA, Gerbi ME et al (2003) Effect of 830-nm laser light on the repair of bone defects grafted with inorganic bovine bone and decalcified cortical osseous membrane. J Clin Laser Med Surg 21:383–388
34. Pinheiro AL, Oliveira MA, Martins PP (2001) Biomodulação da cicatrização óssea pós-implantar com o uso da laserterapia não-cirúrgica: estudo por microscopia eletrônica de varredura (Biomodulation of peri-implant bone repair with laser therapy: SEM study). Rev FOUFBA 22:12–19
35. Silva Junior N, Pinheiro AL, Oliveira MG, Weismann R, Ramalho LM, Nicolau RA (2002) Computadorized morphometric assessment of the effect of low-level laser therapy on bone repair: an experimental animal study. J Clin Laser Med Surg 20:83–88
36. Lopes CB, Pacheco MT, Silveira L Jr, Cangussu MC, Pinheiro AL (2010) The effect of the association of near infrared laser therapy, bone morphogenetic proteins, and guided bone regeneration on tibial fractures treated with internal rigid fixation: a Raman spectroscopic study. J Biomed Mat Res Part A 94:1257–1263
37. Pinheiro AL, Aciole GT, Cangussú MC, Pacheco MT, Silveira L Jr (2010) Effects of laser phototherapy on bone defects grafted with mineral trioxide aggregate, bone morphogenetic proteins, and guided bone regeneration: a Raman spectroscopic study. J Biomed Mater Res A 95:1041–1047
38. Movasaghi Z, Rehman S, Ihtesham U, Rehman IU (2007) Raman spectroscopy of biological tissues. Appl Spectrosc Rev 42:493–541
39. Kirker-Head CA (2000) Potential applications and delivery strategies for bone morphogenetic proteins. Adv Drug Deliv Rev 43:65–92
40. Winn SR, Uludag H, Hollinger JO (1999) Carrier systems for bone morphogenetic proteins. Clin Orthop Suppl 367:S95–S106
41. Cook SD, Baffes GC, Wolfe MW, Sampath TK, Rueger DC (1994) Recombinant human bone morphogenetic protein-7 induces healing in a canine long-bone segmental defect model. Clin Orthop 301:302–312
42. Hunt TR, Hsu HH, Morris DC, Schwappach JR, Lark RG, Anderson HC (1993) Healing of a segmental defect in the rat femur using a bone inducing agent (BIA) derived from a cultured human osteosarcoma cell line (Saos-2). Trans Orthop Res Soc 18:489
43. Reddi AH (1998) Role of morphogenetic proteins in skeletal tissue engineering and regeneration. Nat Biotechnol 16:247–252
44. Nakashima M, Reddi AH (2003) The application of bone morphogenetic proteins to dental tissue engineering. Nat Biotechnol 21:1025–1032
45. Kempen DH, Creemers LB, Alblas J, Lu L, Verbout AJ, Yaszemski MJ, Dhert WJ (2010) Growth factor interactions in bone regeneration. Tissue Eng Part B Rev 16:551–566
46. de Sousa AP, de Aguiar Valença Neto AdeA, Marchionni AM, de Araújo Ramos M, dos Reis Júnior JA, Pereira MC, Cangussú MC, de Almeida Reis SR, Pinheiro AL (2011) Effect of LED phototherapy (λ700±20 nm) on TGF-β expression during wound healing: an immunohistochemical study in a rodent model. Photomed Laser Surg 29:605–611
47. Rocha Júnior AM, Vieira BJ, Andrade LCF, Aarestrup FM (2009) Low-level laser therapy increases transforming growth factor-β2 expression and induces apoptosis of epithelial cells during the tissue repair process. Photomed Laser Surg 27:303–307
48. Saygun I, Karacay S, Serdar M, Ural AU, Sencimen M, Kurtis B (2008) Effects of laser irradiation on the release of basic fibroblastic growth factor (bFGF) insulin like growth factor 1 (IGF-1), and receptor of IGF-1 (IGFBP3) for gingival fibroblasts. Lasers Med Sci 23:211–215
49. Safavi SM, Kazemi B, Esmaeili M, Fallah A, Modarresi A, Mir M (2008) Effects of low-level He-Ne laser irradiation on the gene expression of IL-1β, TNF-α, IFN-γ, TGF-β, bFGF, and PDGF in rat's gingiva. Lasers Med Sci 23:331–335
50. Ihsan FR (2005) Low-level laser therapy accelerates collateral circulation and enhances microcirculation. Photomed Laser Surg 23:289–294
51. Cho HS, Park SY, Kim S et al (2008) Effect of different bone substitutes on the concentration of growth factors in platelet-rich plasma. J Biomater Appl 22:545–557
52. Devescovi V, Leonardi E, Ciapetti G, Cenni E (2008) Growth factors in bone repair. Chir Organi Mov 92:161–168
53. Nandi SK, Roy S, Mukherjee P, Kundu B, De DK, Basu D (2010) Orthopaedic applications of bone graft and graft substitutes: a review. Indian J Med Res 132:15–30
54. Friedman CD, Costantino PD, Takagi S, Chow LC (1998) BoneSource hydroxyapatite cement: a novel biomaterial for craniofacial skeletal tissue engineering and reconstruction. J Biomed Mater Res 43:428–432
55. Reddi AH, Reddi A (2009) Bone morphogenetic proteins (BMPs): from morphogens to metabologens. Cytokine Growth Factor Rev 20:341–342
56. Lissenberg-Thunnissen SN, de Gorter DJ, Sier CF, Schipper IB (2011) Use and efficacy of bone morphogenetic proteins in fracture healing. Int Orthop 35:1271–1280
57. Urist MR, Dowell TA, Hay PH, Strates BS (1968) Inductive substrates for bone formation. Clin Orthop Relat Res 59:59–96
58. Wozney JM (2002) Overview of bone morphogenetic proteins. Spine 27:S2

59. Wang EA, Rosen V, D'Alessandro JS, Bauduy M, Cordes P, Harada T, Israel DI, Hewick RM, Kerns KM, LaPan P et al (1990) Recombinant human bone morphogenetic protein induces bone formation. Proc Natl Acad Sci U S A 87:2220–2224
60. Janssens K, ten Dijke P, Janssens S, Van Hul W (2005) Transforming growth factor-beta1 to the bone. Endocr Rev 26:743–774
61. Desmet KD, Paz DA, Corry JJ et al (2006) clinical and experimental applications of NIR-LED photobiomodulation. Photomed Laser Surg 24:121–128
62. Lanzafame RJ, Stadler I, Whelan HT (2002) NASA LED photoradiation influences nitric oxide and collagen production in wounded rats. Lasers Surg Med Suppl 14:12
63. Tachiara R, Farinelli WA, Rox Anderson R (2002) Low intensity light-induced vasodilation in vivo. Lasers Surg Med Suppl 14:11
64. Vinck EM, Cagnie BJ, Cornelissen MJ, Declercq HA, Cambier DC (2003) Increased fibroblast proliferation induced by light emitting diode and low power laser irradiation. Lasers Med Sci 18:95–99